Ultramicroscopy 110 (2010) 586–591

Contents lists available at ScienceDirect

Ultramicroscopy

journal homepage: www.elsevier.com/locate/ultramic

Atomic force microscopy of silica nanoparticles and carbon nanohorns in macrophages and red blood cells

L. Tetard [a,b], A. Passian [a,b,*], R.H. Farahi [a], T. Thundat [a,b]

[a] Biosciences Division, Oak Ridge National Laboratory, Oak Ridge, TN 37831, USA
[b] Department of Physics, University of Tennessee, Knoxville, TN 37996, USA

ARTICLE INFO

Keywords:
Atomic force microscopy
Mode synthesizing atomic force microscopy
Raman spectroscopy
Nanoparticles
Nanomechanics
Force curves
Cells

ABSTRACT

The emerging interest in understanding the interactions of nanomaterial with biological systems necessitates imaging tools that capture the spatial and temporal distributions and attributes of the resulting nano–bio amalgam. Studies targeting organ specific response and/or nanoparticle-specific system toxicity would be profoundly benefited from tools that would allow imaging and tracking of in-vivo or in-vitro processes and particle-fate studies. Recently we demonstrated that mode synthesizing atomic force microscopy (MSAFM) can provide subsurface nanoscale information on the mechanical properties of materials at the nanoscale. However, the underlying mechanism of this imaging methodology is currently subject to theoretical and experimental investigation. In this paper we present further analysis by investigating tip-sample excitation forces associated with nanomechanical image formation. Images and force curves acquired under various operational frequencies and amplitudes are presented. We examine samples of mouse cells, where buried distributions of single-walled carbon nanohorns and silica nanoparticles are visualized.

1. Introduction

The intersection of biology and nanotechnology presents issues and challenges for both fields. Regardless of whether the nano-bio amalgam was created through undesired exposure [1,2] or directed interaction such as drug delivery [3,4], photothermal ablation [5–7], and in vivo biosensors [6,8,9], a major challenge is the high resolution imaging of a biological system exposed to nanomaterial. As new nanomaterials and uses are being discovered, the need for novel characterization of single cells and single molecules becomes increasingly important to assess the efficacy of nanomedicine and possible adverse health consequences of nanomaterial [10–16].

Quantitative measurements of nanomaterial uptake, biodistribution, and therapeutic/cytoxic effects are an ongoing research effort. Several existing characterization methods play important roles in the overall biological assessment of cells. Optical microscopies, such as confocal fluorescence microscopy, can provide powerful information on the cell–nanoparticle interaction with the use of labeling [7,9,17,18], although individual nanoparticulates are not distinguishable and often high concentrations are required. To identify individual nanomaterials and substructures within cells, transmission electron microscopy (TEM) is frequently employed [8,17–19]. However, the hostile vacuum conditions hamper standard TEM for living systems. Scanning probe microcopy, such as atomic force microscopy (AFM) [20], is a complementary approach that produces nanometer scale resolution and accommodates the living cell in its natural environment [21,22]. Conventional AFM strengths lie in its ability to provide topological and compositional analysis of the surface of the cell, although lacking sufficient sample excitation for accessing subsurface information.

The possibility of combining scanning probe microscopy with acoustic waves in order to perform high resolution near-field imaging (estimated to be around 100 nm) was presented in early work by Akamine et al. [23] on acoustic microscopy. The evolution of ultrasonic probe and/or sample modulation techniques has since revealed remarkable new detail of the specimen, such as elasticity and homogeneity for materials investigation [24,25]. Extending the acoustic excitation in the system to the sample and the probe, it is then possible to access surface and subsurface information on the mechanical properties of materials [26,27]. In particular, the local phase information of the ultrasonic mode resulting from the nonlinear coupling between the forcings on the probe and the sample may be acquired to form the image in a technique known as scanning near field ultrasonic holography (SNFUH) [28]. Using SNFUH, we previously demonstrated the

* Corresponding author at: Oak Ridge National Laboratory, Oak Ridge, TN 37831, USA.
E-mail address: passianan@ornl.gov (A. Passian).

0304-3991/$ - see front matter © 2010 Elsevier B.V. All rights reserved.
doi:10.1016/j.ultramic.2010.02.015

visualization of buried nanoparticles in macrophages and erythrocytes with a resolution of 3 nm [29,30]. By taking advantage of the nanomechanical nonlinear coupling between the probe and the sample of an AFM system, a variety of new modes are now available to probe the subsurface physical properties of materials at the nanoscale, as demonstrated in the newly developed MSAFM [31]. Although preliminary work on modeling the probe-sample interactions have been reported [32–34], the underlying mechanism in the particular case of the ultrasonic microscopy is not fully understood. In this paper, we provide additional results on the image formation stemming from a particular mode of MSAFM, with a frequency that equals the difference $|f_s - f_c|$, by experimentally investigating the tip-sample interaction. This particular mode of MSAFM can be shown to allow comparisons with the previously reported techniques [26–30]. In doing so we analyze probe-sample force curves and images of mouse cells with buried nanoparticles.

2. Experimental procedures

The experimental configuration, shown in Fig. 1, engaged a Veeco AFM, internally consisting of a cantilever, laser, position sensing detector (PSD) and piezoelectric crystal actuation (PZT). Using additional apparatus, the cell and microcantilever probe are oscillated at two different megahertz frequencies f_s and f_c, respectively, with piezoelectric crystals. In the present experiment, the two PZT films (from Physics Instrumente model PIC255) were used to launch longitudinal waves in the system. The ultrasonic excitation of the sample creates propagating waves traveling through the cell that are influenced by the elastic properties of the cell. The experiment was performed in ambient conditions (Fig. 1). The tip-sample coupled oscillations resulting from the two excitations were processed with control electronics and acquired through lock-in detection referenced at the difference frequency, $|f_s - f_c|$ (Fig. 1). The phase contrast of the resulting tip-sample interaction revealed variations in the acoustic impedance throughout the cell, including subsurface structures. A set of frequency, amplitude, and phase settings for sample and probe oscillations are determined from evaluating the quality of the amplitude and phase image. Here we vary the conditions of these parameters in order to engender optimum operation conditions. The resulting tip-sample approach curves with corresponding images were analyzed.

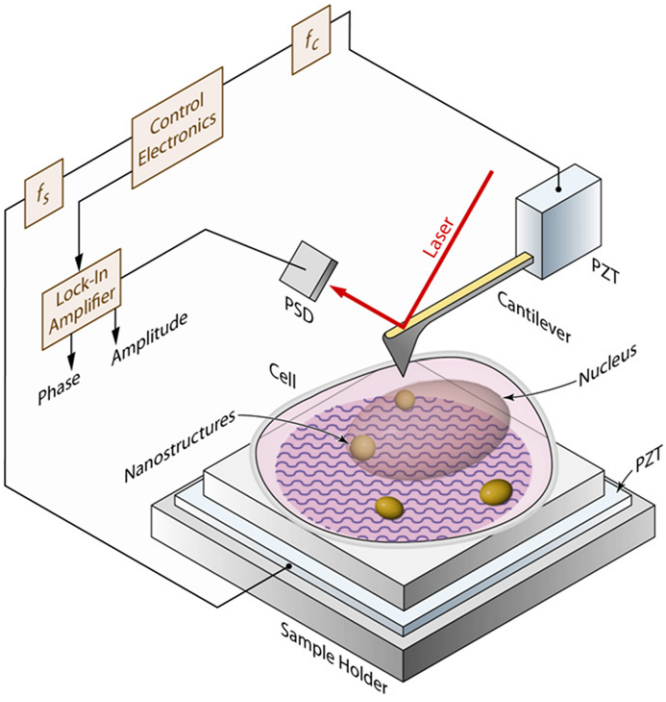

Fig. 1. A schematic of the experimental setup. The probe and sample are oscillated at ultrasonic frequencies f_c and f_s, respectively. The mechanical bending of the cantilever probe represents the nonlinear tip-sample coupling and is measured through laser reflectometry using lock-in amplification referenced at the difference frequency $|f_c - f_s|$. New coupling modes may be created by varying f_c, f_s, and $|f_c - f_s|$.

Samples of alveolar macrophages and erythrocytes (red blood cells) obtained from mice exposed to pluronic-coated single-walled carbon nanohorns (SWCNH) and silica nanoparticles were prepared. Adult male mice from the stocks maintained at ORNL were randomly assigned to two experimental groups: (1) PBS aspiration group and (2) nanoparticle/PBS aspiration group. All mice were housed in the specific pathogen-free facility at ORNL and given water and standard rodent chow ad libitum. The Animal Care and Use Committee at ORNL approved all experimental procedures. Three mice from each group were sacrificed 24 hours after aspiration. Mouse pharyngeal aspiration was used for nanoparticles administration. Aspiration was performed as previously described [29]. Briefly, mice were anesthetized with isoflurane and hung by their incisors on an inclined board. The animal's tongue was extended using forceps, and 30 μL of the control solution or nanoparticle solution was placed on the back of the tongue. The tongue was extended until all of the fluid was aspirated into the lungs.

Mice were sacrificed by isoflurane overdose in a bell jar, and bronchoalveolar lavage (BAL) was performed according to standard protocols. The first lavage was performed with 0.6 ml of PBS and was kept separate for analysis for another study. The second and third lavages were performed with 1.0 ml of PBS and were pooled in sterile tubes, centrifuged, and resuspended in PBS. For light microscopy analysis, cytospin slides were stained with a Hema3 kit (Fisher Scientific). For AFM analysis, cells were centrifuged onto freshly cleaved mica using a cytospin and fixed with methanol. In addition, peripheral blood was collected using heparinized capillaries from the abdominal aorta. Blood samples were diluted in PBS, centrifuged onto freshly cleaved mica using a cytospin, and fixed with methanol.

3. Results and discussion

The cantilever probe motion as a function of time was isolated and examined. Time traces of the motion of the cantilever, the detected signal S(t), is represented in Fig. 2. The first case is a free cantilever, shown in Fig. 2(A), and the second case is where the distance between the probe and the substrate is sufficiently small to generate the nonlinearities in the system, shown in Fig. 2(B). The direct comparison of the traces demonstrates the modulation attributed to the nonlinear coupling between the probe and the sample. The traces presented were recorded at a fixed tip-sample distance. In both cases the cantilever was driven at $f_c = 1$ MHz. The strength of the coupling, that is, the emergence of the peak at $|f_c - f_s|$, is directly dependent on the driving amplitudes of both piezoelectric crystals.

Murine exposure to pluronic-coated SWCNH and silica nanoparticles (see Experimental procedures section) was studied to understand the cellular uptake of these nanomaterials, shown in Figs. 3 and 4. As a control, SWCNHs alone were examined by AFM topography (Fig. 3(A)). The acoustic phase image of the macrophage (Fig. 3(D)) was able to visualize subcellular structures and buried SWCNH that were not detected with AFM (Fig. 3(C)). A closer view of the erythrocytes in Fig. 3(E) showed

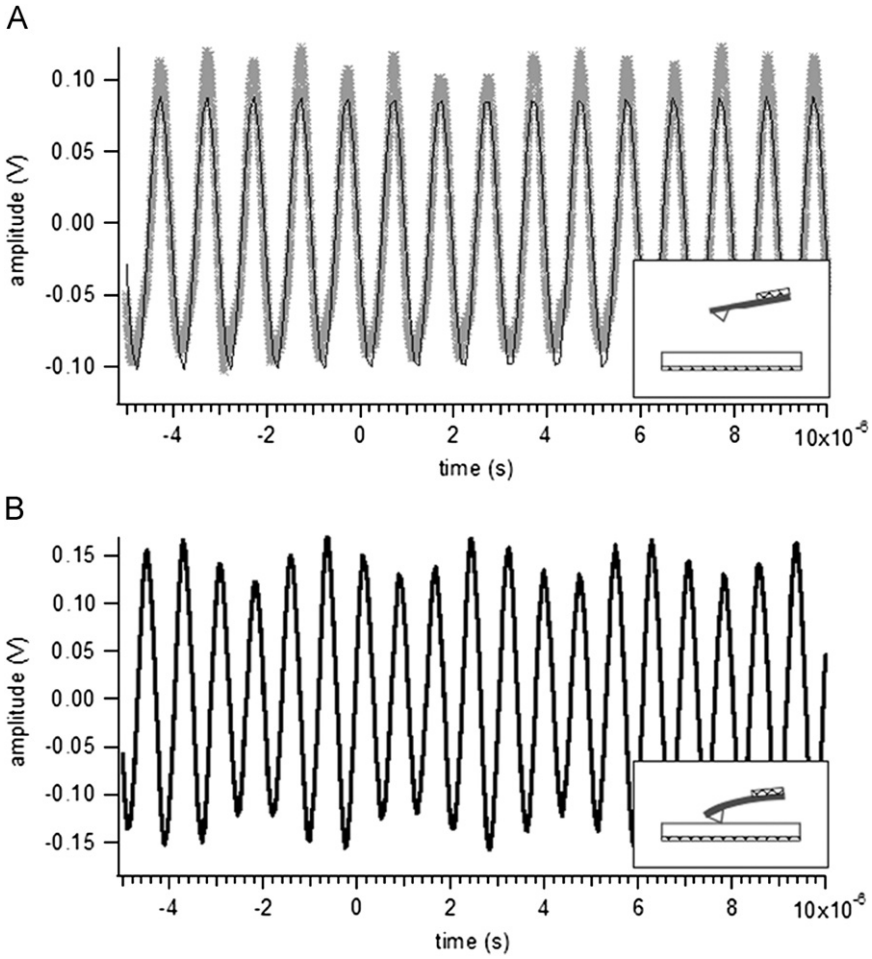

Fig. 2. Time traces representing the motion of the cantilever. As depicted in the insets, (A) the cantilever is free (out of contact with the surface): f_c=1 MHz, a_c=10 Vpp; The black line represents the fit function (sine wave) associated to the measurement (gray line) (B) the cantilever is in contact with the surface and subjected to conditions: f_c=1 MHz, a_c=10 Vpp, f_s=1.3 MHz, a_s=10 Vpp. The amplitude of the motion of the cantilever is modulated as a consequence of the nonlinear coupling between the probe and the surface of the sample.

that SWCNHs could be clearly resolved. The observations were strengthened by the Raman spectroscopy performed on the solution of SWCNH (Fig. 3(B)), the exposed macrophages (Fig., 3(F)), and the exposed erythrocytes (Fig. 3(E)). For instance, the peaks indicative of the presence of the nanoparticles [29] (Fig. 3(A), (B)) were found in the spectra associated to the exposed macrophages (Fig. 3 (C–F)). The results of cellular subsurface localization of the SiO_2 nanoparticles are shown in images in Fig. 4. The average diameter of the particles was measured to be 87 nm. High resolution topographic and phase images consistently resolve individual nanoparticles on the surface of the cell (circled in purple), or within the cell (circled in light blue).

Using macrophage samples exposed to SWCNH, three different excitation forces (frequencies and amplitudes) are presented in Fig. 5. It provides important information on the mechanical behavior of the system for imaging. The force curves are dependent upon the elastic properties of the sample material and the ability of the cantilever to flex in response of the forces (attractive or repulsive) exerted upon the tip and the sample surface. From the measurements presented in Fig. 5, we studied the evolution of the force curves when the driving forces of the system are modified. The results are compared to the force curves originally obtained with standard AFM (no driving force applied). The results reveal an important variation in the response of the system with respect to the different excitations. Note that the mode resulting from nonlinear coupling between the excited probe and sample will be affected by a number of parameters such as the driving amplitude and how close the excitation frequencies of the new modes are from the resonance frequencies of the cantilever. Here we monitor the deflection of the cantilever with respect to the relative displacement of the cantilever holder, either approaching the surface (left) or withdrawing from the surface (right).

The force curves exhibit noticeable differences in the slope of the linear region and the nonlinear region, both in the approach and withdrawal modes. In the three cases presented, the course of the cantilever is identical (1 μm). The distance to the surface when the cantilever jumps in or out of contact is shifted depending on the excitation parameters. In the measurements presented in Fig. 5 the difference frequency varies between 83 kHz (B) and 86 kHz (C). The resonance frequency of the cantilever in contact with the cell sample was determined by sweeping the probe driving frequency from 25 kHz to 1 MHz and recording the corresponding amplitude of the laser reflectometry signal. The resonance frequency was found to be 86 kHz. Fig. 5(C) illustrates the response of the system to the driving frequencies f_s=4.007 MHz and f_c=4.093 MHz. As can be observed on the corresponding acoustic amplitude and phase images, the system became too unstable for imaging purposes. In addition, adhesion increased significantly in this particular case, shown by the relative displacement required for the probe to jump out of contact (see panel corresponding to withdrawal of the probe). The probe responds to the attraction forces earlier than for the other case. Interestingly, given that the driving amplitudes were

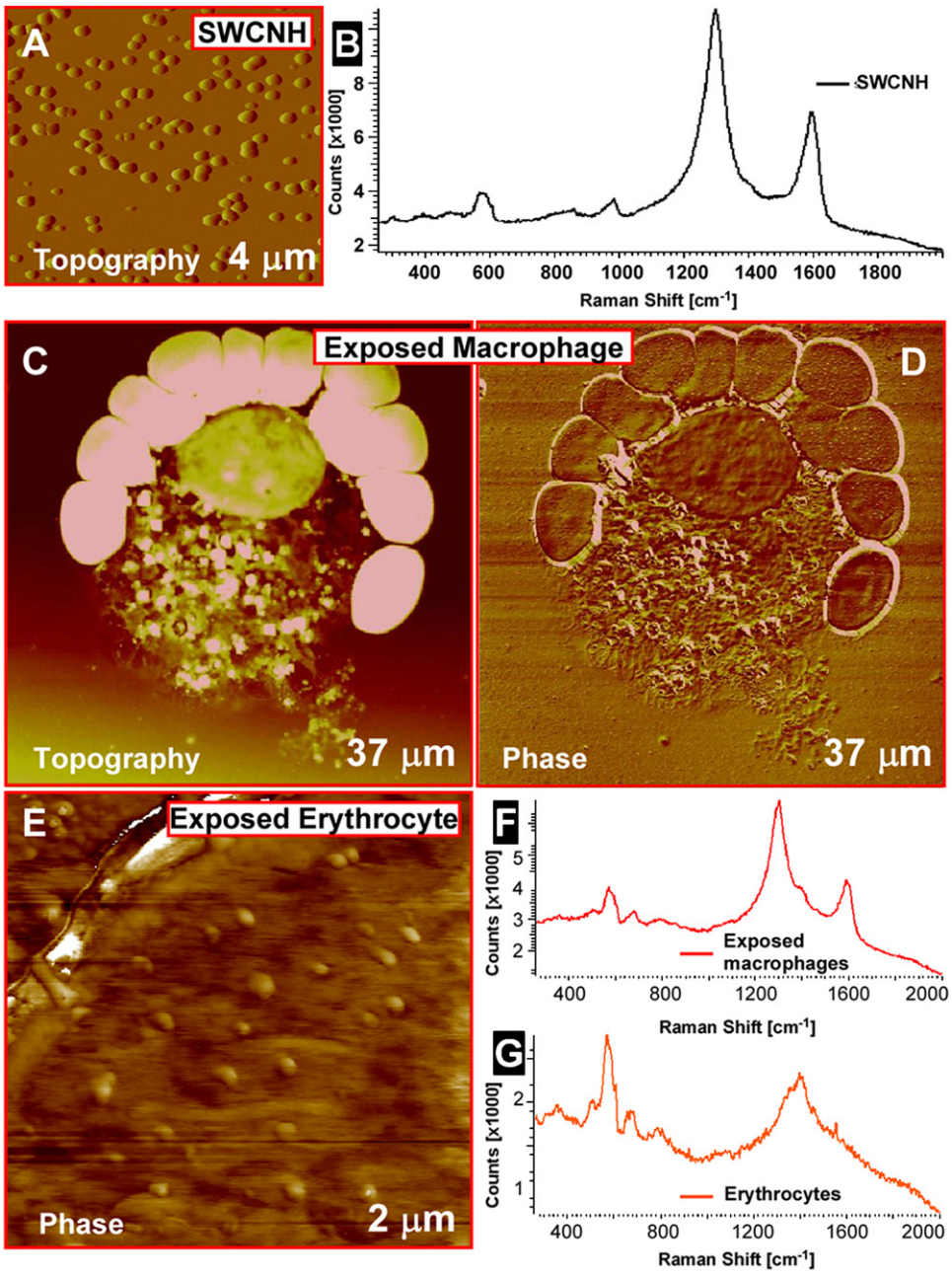

Fig. 3. (A) AFM image of SWCNH on mica and corresponding Raman spectrum (B). (C) AFM image of macrophage exposed to SWCNH. (D) Phase image of macrophage, f_c=4.18 MHz, a_c=3 Vpp, f_s=3.95 MHz, a_s=3.3 Vpp. (E) Phase image of erythrocyte, f_c=4.45 MHz, a_c=2.8 Vpp, f_s=3.95 MHz, a_s=2.2 Vpp. Corresponding Raman spectra of the macrophage exposed to SWCNH (F) and erythrocyte (G).

identical in cases (B) and (C); this behavior can be attributed to the modes generated by the nonlinear coupling and their contribution in the behavior of the cantilever (i.e. the closer to the resonance frequency, the greater the contribution). In the case where the difference in frequency was slightly shifted from the resonance (i.e. Δf=83 kHz (B)), the coupling was satisfactory for imaging. As indicated by the arrows some of the buried SWCNH could then be resolved, but were not visible in (A) or (C). Note that the images remain comparable regardless of whether f_s was greater than f_c or f_c was greater than f_s (not shown here). Note also that in some cases coupling happened to be too weak in order to generate a useful image (not shown here).

Comparing the linear region of the force curves under acoustic excitation to the one obtained for regular AFM, some variations in the slope can be noticed. The dashed lines represent the slope of the force curve in (A). In the case where the coupling was weak, the slope remained unchanged. However in the other cases such as (B) and (C), the material responds differently to the excitations. In (B), the changes translate into the image by providing subsurface information (SWCNH). The elastic properties of the cell, which can be viewed as a network of springs [30] are dependent on the oscillators of the system. The detection of the local coupling was then operated to probe the subsurface cellular information.

4. Conclusion

In summary, we have demonstrated that there is an opportunity to explore new tip-sample excitation forces for MSAFM that

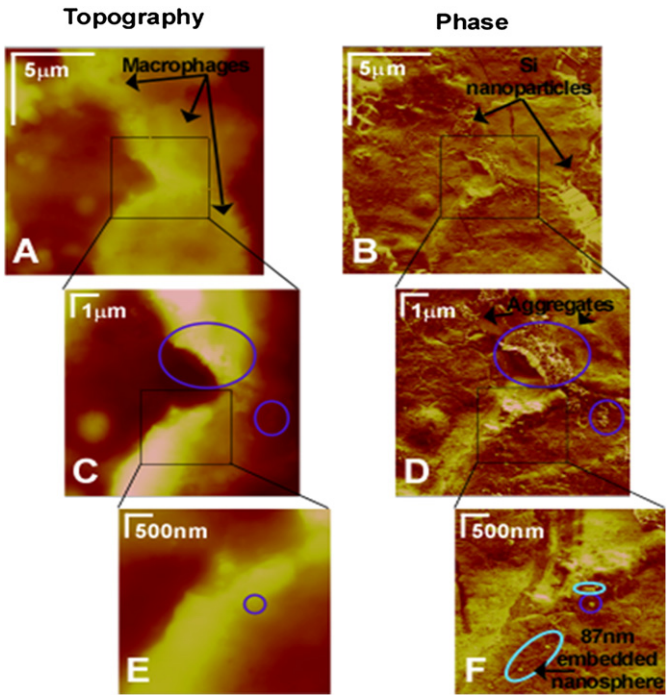

Fig. 4. Images of buried silica nanoparticles in macrophage at different spatial resolution (15, 8 and 4 μm scans). (Left) AFM images. (Right) Phase images. f_c=4.248 MHz, a_c=5.4 Vpp, f_s=3.95 MHz, a_s=2.2 Vpp.

will provide a rich set of characterization data to analyze surface and subsurface features of cells. Using murine macrophages and erythrocytes as test cases, we have obtained images and force curves taken under various operating conditions. Correlating force curves measurements and imaging was important in order to improve the behavior of the system when the probe and the sample are ultrasonically excited. In the present work, we limited our study to the single mode of MSAFM corresponding to $|f_s - f_c|$. However, MSAFM involves a myriad of additional modes, originating from the nonlinear nature of the coupling, and resulting in a very rich but complex dynamics of the system. The force curve measurements presented here reflect the contribution of the various modes. The natural resonance frequencies of the cantilever probe also play an important role in the stability and performance of this new imaging methodology. Furthermore, applying ultrasonic excitations to force spectroscopy may open the path towards measuring new material properties. This high resolution non-invasive imaging modality may be of tremendous potential for characterizing extensive as well as intensive material properties of nano-bio systems without the limitations of current techniques such as special sample preparation/alteration. Within the linear regime, the described nanomechanical imaging preserves the morphological and chemical integrity of the system without electrodynamics or chemical activation/invasion. This is particularly important, as the native fluidic environment of many biological systems, is susceptible to electrodynamics and/or chemical preconditions for other types of probes such as electron bombardment and

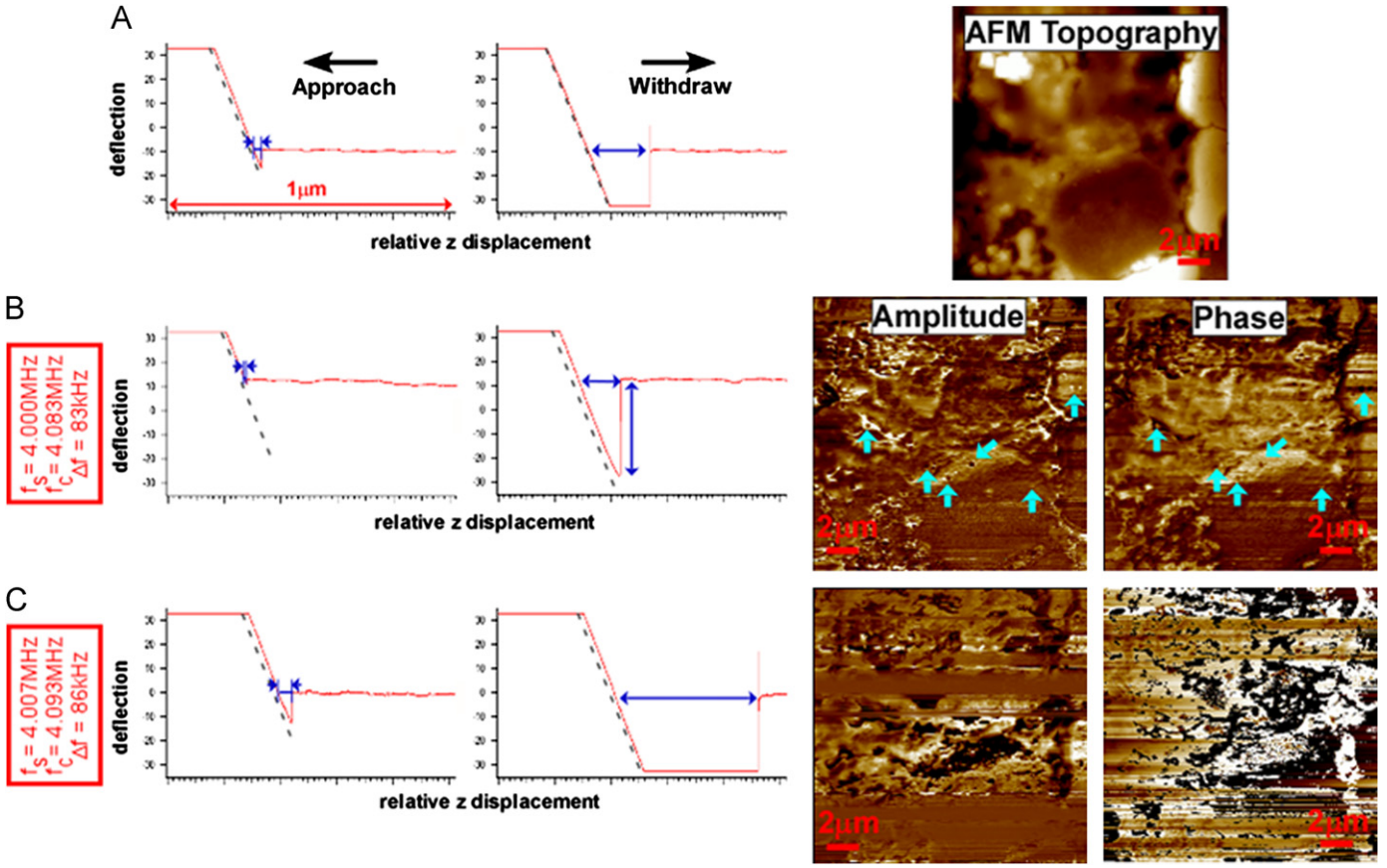

Fig. 5. Influence of the driving frequencies on resulting force curves and phase images. Regular AFM image of a macrophage and resulting force curves (A), (B,C) Amplitude and phase images and corresponding force curves resulting from the probe and sample ultrasonic excitation: (B) f_s=4.00 MHz, a_s=2 Vpp ; f_c=4.083 MHz, a_c=2 Vpp, (C) f_s=4.007 MHz, a_s=2 Vpp ; f_c=4.093 MHz, a_c=2 Vpp. The acoustic images presented are recorded by locking onto (B) 83 kHz, and (C) 86 kHz. The images represent a 20 μm scan size image of the macrophage. The blue arrows in (B) indicate the presence of buried nanoparticles revealed by the technique. (For interpretation of the references to color in this figure legend, the reader is referred to the web version of this article.)

fluorescent tagging. The possibility of extending and adopting such techniques toward the investigation of biological systems is appealing. The principle of operation poses no inherent limitation on the environment in which the imaging occurs, and thus it offers a powerful portal into the imaging of nanoparticles under cellular ambient conditions, that is, in fluid.

Acknowledgements

This research was sponsored in part by the ORNL BioEnergy Science Center. The BioEnergy Science Center is a U.S. Department of Energy Bioenergy Research Center supported by the Office of Biological and Environmental Research in the DOE Office of Science. We are indebted to B.H. Voy and R.M. Lynch at Oak Ridge National Laboratory for providing the samples. We also thank W. Wang and B. Gu for help with Raman spectroscopy. ORNL is managed by UT-Battelle, LLC, for the U.S. Department of Energy under contract DE-AC05-00OR22725.

References

[1] G. Oberdörster, E. Oberdörster, J. Oberdörster, Nanotoxicology: an emerging discipline evolving from studies of ultrafine particles, Environ. Health Perspect. 113 (2005) 823–839.
[2] K. Donaldson, R. Aitken, L. Tran, V. Stone, R. Duffin, G. Forrest, A. Alexander, Carbon nanotubes: a review of their properties in relation to pulmonary toxicology workplace safety, Toxicol. Sci. 92 (2006) 5–22.
[3] K. Ajima, M. Yudasaka, T. Murakami, A. Maigné, K. Shiba, S. Iijima, Carbon nanohorns as anticancer drug carriers, Mol. Pharmaceutics 2 (6) (2005) 475–480.
[4] K. Cho, X. Wang, S. Nie, Z. Chen, D.M. Shin., Therapeutic nanoparticles for drug delivery in cancer, Clin. Cancer Res. 14 (5) (2008) 1310–1316.
[5] L.R. Hirsch, R.J. Stafford, J.A. Bankson, S.R. Sershen, B. Rivera, R.E. Price, J.D. Hazle, N.J. Halas, J.L. West., Nanoshell-mediated near-infrared thermal therapy of tumors under magnetic resonance guidance, PNAS 100 (23) (2003) 13549–13554.
[6] C. Loo, A. Lowery, N. Halas, J. West, R. Drezek, Immunotargeted nanoshells for integrated cancer imaging and therapy, Nano Lett. 5 (4) (2005) 709–711.
[7] J. Chen, D. Wang, J. Xi, L. Au, A. Siekkinen, A. Warsen, Z.-Y. Li, H. Zhang, Y. Xia, X. Li, Immuno gold nanocages with tailored optical properties for targeted photothermal destruction of cancer cells, Nano Lett. 7 (5) (2007) 1318–1322.
[8] G.R. Souza, D.R. Christianson, F.I. Staquicini, M.G. Ozawa, E.Y. Snyder, R.L. Sidman, J.H. Miller, W. Arap, R. Pasqualini, Networks of gold nanoparticles and bacteriophage as biological sensors and cell-targeting agents, PNAS 103 (5) (2006) 1215–1220.
[9] X. Qu, J. Wang, Z. Zhang, N. Koop, R. Rahmanzadeh, G. Hüttmann, Imaging of cancer cells by multiphoton microscopy using gold nanoparticles and fluorescent dyes, J. Biomed. Optics 13 (3) (2008) 031217.
[10] V. Stone, K. Donaldson, Signs of stress, Nat. Nanotechnol. 1 (2006) 23–24.
[11] H.C. Fischer, W.C. Chan., Nanotoxicity: the growing need for in vivo study, Curr. Opin. Biotechnol. 18 (2007) 565–571.
[12] B.J. Panessa-Warren, J.B. Warren, S.S. Wong, J.A. Misewich, Biological cellular response to carbon nanoparticle toxicity, J. Phys. Condens. Matter 18 (2006) S2185–S2201.
[13] T. Xia, M. Kovochich, J. Brant, M. Hotze, J. Sempf, T. Oberley, C. Sioutas, J.I. Yeh, M.R. Wiesner, A.E. Nel, Comparison of the abilities of ambient and manufactured nanoparticles to induce cellular toxicity according to an oxidative stress paradigm, Nano Lett. 6 (2006) 1794–1807.
[14] V.L. Colvin., The potential environmental impact of engineered nanomaterials, Nat. Biotechnol. 21 (2003) 1166–1170.
[15] A.E. Nel, T. Xia, L. Madler, N. Li, Toxic potential of materials at the nanolevel, Science 311 (2007) 622–627.
[16] M. Ferrari, Cancer nanotechnology: opportunities and challenges, Nat. Rev. Cancer 5 (2005) 161–171.
[17] J.M. Wörle-Knirsch, K. Pulskamp, H.F. Krug, Oops they did it again! carbon nanotubes hoax scientists in viability assays, Nano Lett. 6 (2006) 1261–1268.
[18] A. Verma, O. Uzun, Y. Hu, Y. Hu, H.-S. Han, N. Watson, S. Chen, D.J. Irvine, F. Stellacci, Surface-structure-regulated cell-membrane penetration by monolayer-protected nanoparticles, Nat. Mater. 7 (2008) 588–595.
[19] A.E. Porter, M. Gass, K. Muller, J.N. Skepper, P.A. Midgley, M. Welland, Direct imaging of single-walled carbon nanotubes in cells, Nat. Nanotechnol. 2 (2007) 713–717.
[20] G. Binnig, C.F. Quate, C. Gerber, Atomic force microscope, Phys. Rev. Lett. 56 (1986) 930.
[21] P. Parot, Y.F. Dufrêne, P. Hinterdorfer, C. Le Grimellec, D. Navajas, J.-L. Pellequer, S. Scheuring, Review: past, present and future of atomic force microscopy in life sciences and medicine, J. Mol. Recognit. 20 (2007) 418–431.
[22] Y.F. Dufrêne, Towards nanomicrobiology using atomic force microscopy, Nat. Rev. 6 (2008) 674–680.
[23] S. Akamine, B. Hadimioglu, B.T. Khuri-Yakub, H. Yamada, C.F. Quate, Acoustic microscopy beyond the diffraction limit: an application of microfabrication, in: Proceedings of the International Conference on Solid-State Sensors and Actuators, Digest of Technical Papers, Transducers '91, (1991) 857–859.
[24] U. Rabe, W. Arnold, Acoustic microscopy by atomic force microscopy, Appl. Phys. Lett. 64 (1994) 1493–1495.
[25] O.V. Kolosov, M.R. Castell, C.D. Marsh, G.A.D. Briggs, Imaging the elastic nanostructure of Ge islands by ultrasonic force microscopy, Phys. Rev. Lett. 81 (1998) 1046–1049.
[26] O. Kolosov, K. Yamanaka, Nonlinear detection of ultrasonic vibrations in an atomic force microscope, Jpn. J. Appl. Phys. 32 (1993) L1095.
[27] M.T. Cuberes, H.E. Assender, G.A.D. Briggs, O.V. Kolosov, Heterodyne force microscopy of PMMA/rubber nanocomposites: nanomapping of viscoelastic response at ultrasonic frequencies, J. Phys. D: Appl. Phys. 33 (2000) 2347.
[28] G.S. Shekhawat, V.P. Dravid., Nanoscale imaging of buried structures via scanning nearfield ultrasound holography, Science 310 (2005) 89–92.
[29] L. Tetard, A. Passian, K.T. Venmar, R.M. Lynch, B.H. Voy, G. Shekhawat, V.P. Dravid, T. Thundat, Imaging nanoparticles in cells by nanomechanical holography, Nat. Nanotechnol. 3 (2008) 501–505, doi:10.1038/nnano.2008.162.
[30] L. Tetard, A. Passian, R.M. Lynch, B.H. Voy, G. Shekhawat, V.P. Dravid, T. Thundat, Elastic phase response of silica nanoparticles buried in soft matter, Appl. Phys. Lett. 93 (13) (2008) 133113.
[31] L. Tetard, A. Passian, T. Thundat. New modes for subsurface atomic force microscopy through nanomechanical coupling, 10.1038/nnano.2009.454.
[32] R. Garcia, R. Margerle, R. Perez, Nanoscale compositional mapping with gentle forces, Nat. Mater. 6 (2007) 405–411.
[33] N.F. Martinez, S. Patil, J.R. Lozano, R. Garcia, Enhanced compositional sensitivity in atomic force microscopy by the excitation of the first two flexural modes, Appl. Phys. Lett. 89 (2006) 153115.
[34] J.H. Cantrell, S.A. Cantrell, Analytical model of the nonlinear dynamics of cantilever tip-sample surface interactions for various acoustic atomic force microscopies, Phys. Rev. B. 77 (2008) 165409.